TIME TO SURFACE CRACKING AND CRACK WIDTH OF REINFORCED CONCRETE STRUCTURES UNDER CORROSION OF MULTIPLE REBARS

Xun Xi[1, 2] and Shangtong Yang[2*]

[1] *School of Civil and Resource Engineering, University of Science and Technology Beijing, Beijing, 100083, China.*

[2] *Department of Civil and Environmental Engineering, University of Strathclyde, Glasgow, G1 1XJ, United Kingdom.*

ABSTRACT

Concrete cover cracking caused by corrosion of reinforcement is one of major deterioration mechanisms for reinforced concrete structures. In practice, time to surface cracking and crack width evolution are of significance in regards to the assessment of serviceability of reinforced concrete structures. Literature review suggests that, although considerable research has been undertaken on corrosion-induced concrete cracking, little has been focused on corrosion of multiple reinforcing bars, especially by considering the non-uniform corrosion process. In this paper, a time-dependent non-uniform corrosion model is established. A cohesive crack model is then formulated to simulate arbitrary cracking in the whole cover of concrete structures. Two typical cover failure modes (i.e., "delamination" and "combined delamination and corner spalling") have been simulated under the non-uniform corrosion of multiple reinforcing bars and found dependent on spacing of reinforcement and fracture energy of concrete. The effects of corrosion, geometric and mechanical parameters on the time to surface cracking after corrosion initiation and the crack width evolution are also investigated and discussed. The developed model is partially verified by comparing the results with those from experimental tests on uniform corrosion of multiple reinforcing bars.

Keywords: corrosion initiation, surface cracking, non-uniform corrosion, multiple reinforcing bars, cohesive crack model, reinforced concrete, finite element modelling.

* Corresponding author. Tel: +44 141 548 3273. Email: shangtong.yang@strath.ac.uk.

1 INTRODUCTION

Corrosion of reinforcement is a significant problem affecting the durability of reinforced concrete (RC) structures, e.g., bridge decks, retaining walls, piers, tunnels. Practical experience and observations suggest that corrosion-affected RC structures are more prone to cracking than other forms of structural deterioration. Consequently, the corrosion induced cracks destroys the integrity of the concrete cover, deteriorate the bonding strength of the interface between reinforcement and concrete, and lead to premature failure of RC structures. Moreover, the reinstatement cost of corrosion-affected RC structures is significantly high; worldwide, the maintenance and repair costs for corrosion-affected concrete infrastructure are estimated around $100 billion per annum [1].

Considerable research has been carried out in concrete cover cracking induced by corrosion of reinforcement [1-8]. Liu and Weyers [2] were amongst the first to model the surface cracking time of concrete cover due to corrosion of reinforcement, based on a series of experimental tests. Their formula for the critical amount of corrosion products has been widely cited in the research literature. Pantazopoulou and Papoulia [4] established a relationship between the amount of corrosion products and internal pressure from which the cracking time of the concrete cover can be obtained. Li *et al.* [9] developed an analytical model to calculate the crack width of concrete cover caused by corrosion of reinforcement. Amongst these existing studies, most are focused on uniform corrosion of a single reinforcing bar.

However, due to the fact that chlorides, as well as moisture and oxygen, penetrates into surface of steel at different rates on different sides of the concrete, it is rare to have a uniform corrosion on the reinforcing bar. Recently, some researchers have started to model the cracking of concrete cover induced by non-uniform corrosion. According to geometry and diffusion properties of concrete, non-uniform corrosion model can be built by considering chloride concentration via Fick's second law of diffusion [10-12]. However, the actual environmental conditions of concrete may differ significantly from the hypothesis under Fick's law [13]. Meanwhile, experimental tests or field surveys have been carried out to determine the distribution of corrosion rust which is found not uniform along the circumference of the reinforcement [14-16]. Almost all the experimental results in literature have shown that only the part of reinforcement facing concrete cover is corroded and the further towards the concrete surface the location is, the more corrosion products that are produced at this location. Some studies introduced a factor defining the ratio of the depth of non-uniform corrosion to that of uniform corrosion, and found that its value ranges about 4-8 in natural conditions [17-19]. Yuan and Ji [16] conducted corrosion tests on reinforced concrete samples in an artificial environmental chamber and found that, only a half of the reinforcement, facing concrete cover, was corroded and the expansion was in a semi-elliptical shape. Similar corrosion distributions were also found in other experiments [20].

Moreover, corrosion rate is the most important single parameter controlling the corrosion development [2, 9, 21, 22]. Previous work on predicting of corrosion-induced cover cracking mainly assumes a constant mean annual value of corrosion rate for the whole life-cycle of RC structures after corrosion initiation [18, 19, 23]. However, the corrosion process of steel reinforcing bar is an electrochemical reaction process influenced by three factors, i.e., chloride concentration, oxygen content and resistivity of concrete [24]. In natural environment, the actual corrosion rate should change throughout the year and the full life-cycle of RC structures. A number of researches have been made to analytically establish the corrosion rate model for the entire lifetime of RC structures based on the electrochemical theory and/or to conduct experiments under artificial and nature climate environment conditions for verifications [25-28].

Under the expansive force caused by non-uniform corrosion of reinforcement, concrete cover can be cracked which leads to delamination of the cover. To investigate the structural effects of corrosion on the concrete cover, most previous work is focused on a single reinforcing bar, e.g., in [11, 18, 29]. It has been proved that the location of rebar (i.e., corner and middle rebars, respectively) and boundary conditions have significant effect on cover cracking induced by reinforcement corrosion [11, 29]. Moreover, spacing between the reinforcement, in case of multiple reinforcing bars, can influence the stress fields and thus the time to surface cracking and the cracking patterns. Very few of the existing models can well explain the effect of corrosion of multiple rebars on cracking of the whole concrete cover, including those of uniform corrosion [30]. Amongst the limited studies on corrosion of multiple rebars, Chen et.al [19] simulated the crack patterns of concrete cover induced by uniform corrosion of two reinforcing bars via lattice model. Further, Zhang et.al [31] modelled the cover cracking of RC structures with two reinforcing (middle) bars under non-uniform corrosion via damage plastic model. Literature review suggest that very little work has been carried out on cover cracking induced by non-uniform corrosion of multiple reinforcing bars of RC structures and; the relationship between the cover cracking and the time-dependent corrosion rate of the whole life-cycle under corrosion of multiple reinforcing bars has not been established.

This paper attempts to develop a combined analytical and numerical method to predict the time to cover cracking after corrosion initiation and the crack width under time-dependent non-uniform corrosion of multiple reinforcing bars of RC structures. A non-uniform corrosion model is first formulated based on available experiment results. The time-dependent corrosion rate in the whole life-cycle of RC structures is introduced. Under the expansion caused by corrosion of multiple reinforcing bars, arbitrary discrete cracks are modelled in cover concrete by cohesive elements with finite element method. Time to concrete cracking, crack width and crack patterns of the whole cover are obtained. The developed model is partially verified by comparing the results of uniform corrosion from the developed method and experiments, due to the lack of experimental data on non-uniform corrosion. Moreover, a parametric study is carried out to investigate the effects of some key parameters, e.g., fracture energy of concrete, spacing between the reinforcing bars and corrosion rate, on the time to surface cracking and crack width, under non-uniform corrosion of multiple reinforcing bars.

2 RESEARCH SIGNIFICANCE

Considerable research has been conducted in the last few decades in modelling corrosion of reinforcement in concrete and its effects on concrete cover cracking. However, most of existing studies are focused on corrosion of a single reinforcing bar and model the cover cracking as a thick-wall cylinder (mainly analytical) or other geometries (mainly numerical). Very few models could address the interactive behaviour of corrosion of multiple reinforcing bars of RC structures, e.g., beams with 4 tensile rebars. In fact, the cover cracking patterns, time to surface cracking and crack width development could be significantly affected by the combined stress fields generated from corrosion of multiple steel bars. Therefore, a rational model for predicting concrete cover cracking should employ a system approach, by considering all corrosion-affected reinforcing bars, rather than a simplified approach by simulating a single bar only. Moreover, corrosion is actually a time-dependent process and non-uniform along the circumference of reinforcing bars. It would be ideal to derive a time-dependent non-uniform corrosion model for failure prediction of the whole cover of RC structures with multiple reinforcing bars. It is in this regard this paper is presented.

3 TIME-DEPENDENT NON-UNIFORM CORROSION

Chloride-induced corrosion of reinforcing bar in concrete produces rusts (mainly ferrous and ferric hydroxides, $Fe(OH)_2$ *and* $Fe(OH)_3$) which accumulate and result in cracking, spalling and delamination of RC structures. The corrosion rusts first fill in the annular porous layer in concrete around the reinforcing bar, often referred to "diffusion zone" or "porous zone". This initial stage normally does not produce stresses in concrete. As schematically shown in Figure 1, D is the diameter of the bar and d_0 is thickness of the "porous zone". The thickness d_0 varies from 10 to 20 μm according to the porosity of concrete and compaction degree, which is constant once concrete has hardened [23]. Depending on the level of corrosion, the products of corrosion may occupy up to a few times more volume than the original steel. As corrosion of the reinforcement propagate further, a band of corrosion products forms, as shown in Figure 1. If corrosion process is assumed uniform, the band becomes a circular ring which causes uniform stresses in the concrete. However, due to the fact that the chlorides, as well as moisture and oxygen, reach the reinforcement surface at different rates through top side of the concrete structure, it is rare to have uniform corrosion around the reinforcement. Experiments results suggest that the front of corrosion products for the half of rebar facing concrete cover is in a semi-elliptical shape, while corrosion of the opposite half of rebar is negligibly small [16].

As illustrated in Figure 1(b), the total amount of corrosion products W_{rust} can be assumed to occupy three bands: the semi-elliptical band of corroded steel with maximum thickness d_{co-st}, the porous circular band d_0 and the semi-elliptical rust band with maximum thickness d_m. The semi-major axis and semi-minor axis for the semi-ellipse of corrosion front are $D/2+d_0+d_m$ and $D/2+d_0$, respectively.

Based on the geometry, the total amount of corrosion products W_{rust} can be shown as follows:

$$\frac{2W_{rust}}{\pi}\left(\frac{1}{\rho_{rust}}-\frac{\alpha_{rust}}{\rho_{st}}\right)=Dd_0+d_0^2+\frac{D}{2}d_m+d_0d_m \tag{1}$$

where α_{rust} is the molecular weight of steel divided by the molecular weight of corrosion products. It varies from 0.523 to 0.622 according to different types of corrosion products [2]. ρ_{rust} is the density of corrosion products and ρ_{st} is the density of steel.

By neglecting the second order of small quantities, i.e., $d_0 d_m$ and d_0^2, d_m can be derived as follows:

$$d_m = \frac{4W_{rust}}{\pi D}\left(\frac{1}{\rho_{rust}} - \frac{\alpha_{rust}}{\rho_{st}}\right) - 2d_0 \tag{2}$$

To determine the displacement boundary condition caused by the rust expansion of the rebar, the function of the semi-ellipse of the corrosion front in rectangular coordinate system can be expressed as follows:

$$\frac{y^2}{\left(\frac{D}{2} + d_0 + d_m\right)^2} + \frac{x^2}{\left(\frac{D}{2} + d_0\right)^2} = 1 \tag{3}$$

Equation (3) can be transformed in a polar coordinate system. By considering the original location of inner boundary of the concrete, i.e., $D/2 + d_0$, the displacement boundary condition can be derived as follows,

$$r = \frac{(D + 2d_0 + 2d_m)(D + 2d_0)}{\sqrt{(2D + 4d_0)^2 + 16d_m(D + 2d_0 + d_m)\cos^2\theta}} - \frac{D}{2} - d_0 \tag{4}$$

where $0 \le \theta \le \pi$.

By substituting Equations (2) in to Equations (4), the displacement boundary condition of concrete $\delta(\theta, t)$ can be derived as follows:

$$\delta(\theta,t)=\frac{\left[D+2d_0+\frac{8W_{rust}(t)}{\pi D}\left(\frac{1}{\rho_{rust}}-\frac{\alpha_{rust}}{\rho_{st}}\right)-4d_0\right](D+2d_0)}{\sqrt{(2D+4d_0)^2+32\left[\frac{2W_{rust}(t)}{\pi D}\left(\frac{1}{\rho_{rust}}-\frac{\alpha_{rust}}{\rho_{st}}\right)-d_0\right]\left[D+2d_0+\frac{4W_{rust}(t)}{\pi D}\left(\frac{1}{\rho_{rust}}-\frac{\alpha_{rust}}{\rho_{st}}\right)-2d_0\right]\cos^2\theta}}-\frac{D}{2}-d_0 \tag{5}$$

where $0 \le \theta \le \pi$.

In Equations (5), $W_{rust}(t)$ is related to the corrosion rate of the steel bar and can be expressed as follows [2]:

$$W_{rust}(t)=\sqrt{2\int_0^t 0.105(1/\alpha_{rust})\pi D i_{corr}(t)dt} \tag{6}$$

$W_{rust}(t)$ is the total amount of rust products at time *t*. i_{corr} is the corrosion current density and t is time after corrosion initiation. The units of these variables are presented in Tables.

As described in Equations 5 and 6, the corrosion rate i_{corr} can be the most important single factor controlling the amount of corrosion products which determines the displacement boundary condition of concrete. Based on previous studies on experiments and simulations in terms of corrosion initiation, corrosion propagation and cover cracking [13, 24, 26, 32-34], etc., the corrosion process of steel bar in concrete for the whole life-cycle could be divided into six stages: (1) no corrosion—chloride ions penetrate the concrete cover and reach to the threshold value; (2) corrosion initiation—gradual depassivation process of the steel bar; (3) corrosion products free expansion—the oxygen and moisture supply in the “porous zone” gradually reduce while the rust occupies the “porous zone”; (4) steady corrosion—the equilibrium between consuming and transporting oxygen and moisture is maintained; (5) accelerated corrosion— caused by significant cracking which leads to faster transport of oxygen and moisture; and (6) final steady corrosion—the reinforcing bar exposes to chloride and atmosphere directly. The development of corrosion rate in the whole life-cycle of RC structures can be schematically shown in Figure 2.

This paper mainly focuses on the time from corrosion initiation to surface cracking (crack width smaller than 0.3-0.6mm). The time needed for chlorides to penetrate the concrete to the depth of the reinforcement (i.e., Stage 1) is excluded. Since stage 2 is usually very short and stages (5) and (6) are normally beyond the serviceability of RC structures, the corrosion rate for the stages (3) and (4) in the whole life-cycle of RC structures can be expressed as follows [27]:

$$i_{corr} = \frac{1}{2}\delta\left\{3\times10^{-2}\exp[9500(\frac{1}{298}-\frac{1}{T})]\right\}^{0.5}\left\{1\times10^{-3}\exp[2612(\frac{1}{T}-\frac{1}{298})]\right\}^{0.5}\exp[\frac{(522+1.44T)}{\beta(t,R_{con})}] \quad (7)$$

$$\beta(t,R_{con}) = \begin{cases}[143.78-54\times(w/c)+0.018R_{1,con}]+[0.78-0.92\times(w/c)-1.2\times10^{-4}R_{con}]\times t,(t_1 \le t < t_2)\\ [143.78-54\times(w/c)+0.018R_{1,con}]+[0.78-0.92\times(w/c)-1.2\times10^{-4}R_{con}]\times t_2,(t_2 \le t < t_3)\end{cases}$$

where δ is the ratio of activation area to the total surface area, which is 0.5 in the non-uniform corrosion model; T is the absolute temperature of concrete, which can be considered as the same as the ambient temperature due of the lack of true temperature data of the internal concrete; $\beta(t,R_{con})$ is the natural logarithm Tafel slopes of the polarization curve. w/c is the water cement ratio; t_1, t_2 and t_3 are times illustrated in Figure 2. At t_2, the amount of corrosion products $W_{rust}(t_2)$ fully fills in the "porous zone", with the thickness d_0; therefore, Equation (1) can be re-written as follows,

$$\frac{2W_{rust}(t_2)}{\pi D}\left(\frac{1}{\rho_{rust}}-\frac{\alpha_{rust}}{\rho_{st}}\right) = d_0 \quad (8)$$

t_2 can be determine by combining the Equations (6) and (8). In Equation (7), R_{con} is the resistivity of concrete, which is related to water cement ratio w/c, chloride content Cl^-, temperature T and pore water saturation P, with the expression presented as follows [27]:

$$R_{con} = [750{,}605 \times (w/c) - 106{,}228] \times \exp[-44.17 \times Cl^- - 7.7213 \times P + 2889(\frac{1}{T} - \frac{1}{303})] \quad (9)$$

$R_{1,con}$ is the resistivity of concrete at time t_1.

It has been found that surface chloride concentration does not change significantly with time for most RC structures in coastal zone [13]. Moreover, numerical simulations on chloride diffusion indicated that after corrosion initiation, the chloride content in concrete will not increase significantly given constant value of surface chloride concentration under natural environment [35]. The pore water saturation P is related to internal relative humidity and temperature. Although the relative humidity and temperature in nature climate changes considerably, pore water saturation P does not change much because of the response hysteresis of concrete to external climate [28]. Therefore, temperature could be the most significant factor that affects the corrosion rate after corrosion initiation in concrete under an atmospheric environment. Similar statements have been found in previous literatures, e.g. [28, 35].

4 COVER CRACKING MODEL

Concrete is modelled as a quasi-brittle material, with its constitutive tensile stress-displacement relation ($\sigma - \delta$) illustrated in Figure 3. To model the arbitrary cracking in concrete, cohesive elements are embedded in the mesh which is sufficiently fine. The insertion process of cohesive elements is shown in Figure 4. First, all individual nodes are replaced by certain number of new nodes at the same location. The number of newly created nodes depends on the number of the elements connecting to the original node. Second, the newly created nodes at the interface between two triangle elements are identified and linked to form a cohesive element. The cohesive elements are shown in red in Figure 4. This insertion process was conducted by a script written in Python. Moreover, it should be mentioned that the cohesive elements generated are of zero thickness in geometry. The two nodes of a cohesive element, in the thickness direction, share the same coordinates before loading. The constitutive/calculation thickness of the cohesive elements, however, is 1.0 for the convenience of transformation between strain and displacement.

Figure 5 shows a RC beam with four tensile reinforcing bars and two compressive reinforcing bars. In light of reducing the computing time, only half of the structure is modelled due to the symmetry of the structure and the loading, as illustrated in Figure 5. The beam is modelled in 2D since it is a plane strain problem. Two elements are employed in this study, i.e., 4-node cohesive elements at all interfaces between the triangle solid elements, and 3-node plane strain element for the bulk intact concrete. The size of solid elements in the region close to the corrosion products varies from 0.6 mm to 1.5 mm while the size in other region varies from 1.5 mm to 15 mm. Very fine mesh is generated before inserting sufficient number of cohesive elements. The meshed structure is shown in Figure 6. There are 12,040 solid triangle elements and 17,865 cohesive elements inserted, for half of the structure with clear spacing between tensile rebars of 30 mm. The expansive behaviour of non-uniform corrosion is modelled by applying radial expansive displacement to the concrete structure.

5 RESULTS AND VALIDATION

5.1 Worked example

To demonstrate the application of the derived method, the time-dependent corrosion rate is first calculated. The average monthly temperature in England from 1996-2016 is used which is listed in Table 1 [36]. According to the data in Table 1, the temperature can be analytically formulated and expressed as a function of time:

$$T = -5.98 \times \cos((t - 0.5) \times (2\pi)) + 10.39 \tag{10}$$

where T is in Centigrade and should be transformed to absolute temperature to calculate the corrosion rate in Equation 7. t is the time in year.

With the values for input parameters shown in Table 2 the corrosion rate for the whole life-cycle from corrosion initiation to surface crack width up to 0.3-0.6 mm can be obtained and shown in Figure 7. It should be noted that the initial increase of corrosion rate, i.e., stage 2 in Figure 2, is neglected in the whole life-cycle analysis in this study since the period is negligibly small. It can be seen that, in the free expansion stage, the corrosion rate i_{corr} decreases from 1.69 to 1.07 μA/cm^2, and the "porous zone" is fully filled with the corrosion products. This process takes about 0.07 year. As discussed, the reason for the drop of corrosion rate is because the consumption of oxygen in the "porous zone". In the steady corrosion stage, the fluctuation of corrosion rate is caused by the seasonal variation of temperature. The lowest corrosion rate is 0.63 μA/cm^2 and the highest is 1.1 μA/cm^2.

After calculating the time-dependent corrosion rate, the maximum non-uniform corrosion induced expansive displacement $d_m(t)$, as illustrated in Figure 1, can be shown as a function of time after corrosion initiation in Figure 8. For better evaluating the time-dependent corrosion rate, developments of corrosion expansion $d_m(t)$ under three constant corrosion rates ($i_{corr} = 0.5$, 1.0 and 2.0 μA/cm^2) are plotted. First, it has been found that the growth curves of $d_m(t)$ over time for constant corrosion rates are rather smooth while that for the time-dependent corrosion is slightly fluctuating. This is because the model proposed in this paper for corrosion rate is a function of temperature which changes during a year. The $d_m(t)$ curve for the time-dependent corrosion rate initially falls in between the curves for $i_{corr} = 1.0$ μA/cm^2 and 2.0 μA/cm^2, respectively; after about 0.4 year, however, the time-dependent curve progresses below the curve for $i_{corr} = 1.0$ μA/cm^2. Therefore, it would be hard to find any constant corrosion rate to represent the time-dependent corrosion rate in terms of the development of corrosion induced expansion over time. This also justifies the use of time-dependent corrosion rate rather than constant corrosion rate. For the time-dependent corrosion rate, corrosion starts to cause stress/displacement onto concrete at 0.07 year.

5.2 Cover failure modes

A number of combinations of reinforcement clear spacing (S) and fracture energy of concrete (G_f) are modelled in this study to investigate the cover failure patterns caused by corrosion of multiple reinforcements. Three values of the reinforcement spacing (S), i.e., 30 mm, 45 mm and 60 mm, and three fracture energy of concrete (G_f) 60 N/m, 90 N/m and 120 N/m, are used. The geometric and mechanical parameters of the RC structures are shown in Table 3. There are two typical failure patterns of the cover structure which have been found. The cracking patterns and time to cracking for different combinations of reinforcement spacing (S) and fracture energy of concrete (G_f) are presented in Table 4. As shown in Figure 9, the first pattern has a through crack between reinforcing bars and a side crack whilst no top crack is visible. Such a pattern is considered as a delamination failure of the cover. For the other pattern, however, there is a top crack above the side reinforcing bar, other than the through crack and the side crack. This pattern tends to cause spalling of the corner concrete cover and hence it is regarded as a combined delamination and corner spalling failure of the cover. In general, relative small values of reinforcement spacing and fracture energy of concrete tend to cause typical delamination failure of concrete cover while high values of these two parameters tend to lead to spalling failure of concrete corner. Discussions on the effects of reinforcement spacing and fracture energy of concrete on the cover failure will be presented in Section 6.

5.3 Verification

The derived model is verified by comparing the time to surface cracking with experiments from literature [37]. According to the literature searched, almost all the test data regarding to the time to cracking for multiple reinforcement corrosion are based on uniform corrosion development by electric current method for accelerated corrosion [32, 37, 38]. As such, a special numerical case on uniform corrosion is conducted and the results are compared with those from experiments [37]. The same inputs from the tests are used in the numerical simulation, which are presented in Table 5. The correlation between the time and uniform corrosion expansion is achieved by the corrosion model presented in Li and Yang [1]. The comparisons of crack width for the side reinforcing bar between the developed model and the experimental results are illustrated in Figure 10. It can be found that the progress of crack width simulated is in reasonably good agreement with the experimental results. The time to surface cracking in the experiment is 72 hours, which is very close to the time when crack width reaches 0.02mm from the simulation. It should be mentioned that, in the experiment, the measured time to crack initiation and propagation is calibrated as it was for corrosion rate 100 $\mu A/cm^2$ and the surface crack initiation is obtained by a crack detection microscope with an accuracy of 0.02mm.

5.4 Justification of top crack

It is very interesting to find that, in the combined delamination and corner spalling failure mode, the top crack always starts from the outer surface and propagates inwards to the reinforcing bar. This is different from the common perspective on corrosion-induced cracking which is usually considered to be initiated from inside to outside of the concrete cover.

Similar results have been found in experimental tests from S. Caré *et al*. [39] and damage simulations from Du *et al*. [29] which indicated that a vertical crack was generated at surface of concrete and propagated towards the rebar. To thoroughly investigate this problem, the stress distributions (maximum principal stress) of the corner rebar region under uniform corrosion and non-uniform corrosion respectively are plotted in Figure 11. It can be found that, for uniform corrosion, the maximum principal stress concentrates around the reinforcement in a relative uniform manner. By sign convention, the maximum principal stress is tensile stress. The maximum principal stresses for all elements in this region are tensile stresses while largest stress occurs at the inner boundary, according to Figure 11 (a). This is why the uniform corrosion-induced crack is always initiated at the inner boundary. For the non-uniform corrosion developed from this study, the stress concentrates around two sides of the inner boundary — roughly at 10 degrees above the horizontal direction, as illustrated in Figure 11 (b). This is where the side crack is initiated; after that, the side crack propagates towards the side surface. A closer look is shown in Figure 12 (a) in which a tensile stress concentration is clearly demonstrated. However, for the potential top crack, the inner boundary region is in bi-axial compression, as illustrated in Figure 12 (b). It is therefore impossible to have a crack initiated here. However, at the top surface, the region is in tension in the x-direction where the top crack should start. The different stress distributions for uniform and non-uniform corrosion models determine the cracking patterns of the concrete cover and explain why the non-uniform corrosion induced top crack is initiated from the top surface, rather than from the inner boundary of concrete cover.

6 ANALYSIS AND DISCUSSION

6.1 Corrosion parameters

Corrosion rate has been considered as one of the key factors affecting the durability of reinforced concrete structures. The effect of constant corrosion rates on time to surface cracking for the model (spacing of reinforcement 45 mm and fracture energy 90 N/m) is investigated and shown in Figure 13. It can be found that the increase of corrosion rate reduces the time to surface cracking. For relatively low corrosion rate, e.g., i_{corr} is smaller than 1.0 μA/cm^2, the time to surface cracking decreases sharply from 7.5 years to 0.75 year. However, for moderate or high rate of corrosion, e.g., i_{corr} is larger than 1.0 μA/cm^2, the time to surface cracking does not change dramatically.

One of the advantages of the corrosion model developed in this paper is that the corrosion rate is directly related to ambient temperature and chloride content in concrete cover. To investigate the effect of temperature on the time to surface cracking, values of temperature in range of 5-35°C are used to calculate the constant corrosion rates. The time to surface cracking for the model (spacing of reinforcement 45mm, fracture energy 90N/m and chloride-ion content 3.034%) as a function of temperature is shown as Figure 14. It can be seen that, the concrete cover surface cracking is advanced from about 1.5 years to 0.2 year, as the temperature changes from 5°C to 35°C. This proves that the time to surface cracking is very sensitive to temperature. However, it has also been found the surface cracking is more sensitive to changes of temperature lower than 25°C, than that of temperature higher than 25°C.

The effects of chloride content in concrete on the cracking of concrete cover have also been investigated which is shown in Figure 15. As expected, the time to surface cracking is reduced as the content of chloride ions increases. When chloride ions content is increased from 1% to 4%, the time to surface cracking is advanced from 2.17 years to 0.84 year. After

4% chloride concentration up to 7% investigated, the decrease in time to surface cracking is only 0.23 year down to 0.61 year. Therefore, it can be postulated that the cracking of concrete cover is very sensitive to the change of low chloride concentrations up to 4%.

6.2 Crack width

To investigate the effect of corrosion rate on evolution of surface crack width, the model for spacing of reinforcement 30 mm and fracture energy 60 N/m is taken as an example based on time-dependent corrosion rate and three constant low/moderate corrosion rates, i.e., $i_{corr} = 0.5$ μA/cm^2, $i_{corr} = 1.0$ μA/cm^2 and $i_{corr} = 2.0$ μA/cm^2. The crack width is obtained by measuring the distance between the nodes of the cohesive element at surface of concrete cover. It should be noted that, before the surface cracking, i.e., cohesive element being deleted, the cohesive element already has a deformation according to the constitutive definition of the cohesive elements. This displacement should be disregarded from the crack width calculation. As illustrated in Figure 16, the increase of corrosion rate can cause significant reduce in time to surface cracking. The initial sudden increases in the surface crack width for different corrosion rate are almost the same since the geometry and mechanical parameters in these models are the same. Further, higher corrosion rate can result in considerably larger surface crack width than lower corrosion rate, for long-term crack width growth. It should be mentioned that since the corrosion mechanism will change significantly after the crack width larger than 0.3 mm [26] which is not considered in the developed model, only 10-year service life is investigated in which the crack widths for most cases are smaller than 0.25 mm.

The effects of the fracture energy on development of side and top surface cracks are shown as Figures 17 and 18. In Figure 17, it can be seen that larger fracture energy of concrete will delay the time to side surface cracking and cause larger initial sudden increase in the crack width. However, the differences in time to surface cracking and initial crack width development are both very small. Moreover, the long-term developments of the crack width for these two cases investigated are almost identical. Figure 18 illustrates the effect of the fracture energy of concrete on the development of top surface crack width. Similarly, larger fracture energy of concrete will result in larger initial increase of crack width and longer cracking time. The fracture energy of concrete has little effect on the long-term development of top surface crack width. It is interesting to find that, when the through crack completely forms, there is a sudden drop in top surface crack width. Such an effect of formation of through crack on the surface crack growth has not been found in previous literatures.

The effect of spacing between reinforcing bars S on the top surface crack width is shown in Figure 19. Fracture energy 120 N/m is used in this analysis. It can be found that the initial crack width growth is significantly affected by the spacing between reinforcements while the long-term developments of crack width are almost the same. Further, there is a sudden drop of crack width for S = 60 mm which is caused by the complete formation of the through crack. As explained, when the through crack is formed, there will be a sudden energy release which leads to unloading of the other cracks. There is no drop for S =30 and 45mm because the through crack forms ahead of the initiation of the top crack.

6.3 Cracking time

Although the through crack is an internal crack which can be less important in terms of the durability, it has significant effects on the development of surface cracks, i.e., the side and top cracks. Figure 20 (a) shows the effects of fracture energy of concrete and spacing between reinforcing bars on time to complete formation of through crack. It can be seen that the larger the fracture energy of concrete or the spacing between reinforcements is, the longer the time to formation of through crack is. Moreover, the effects of fracture energy of concrete and spacing between reinforcing bars on time to initiation of top crack are shown in Figure 20 (b). Only results of S = 45 and 60 mm are plotted because there is no top crack for most cases of S = 30 mm, i.e., delamination mechanism in Figure 9. Again, it has been found that the increase of fracture energy of concrete can delay the time to initiation of top crack. In addition, the effect of spacing is very sensitive, for larger fracture energy of concrete. For fracture energy 60 and 90N/m, there are almost no differences between cases of S = 45 and 60 mm, whilst the time to initiation of top crack is nearly doubled for fracture energy 120N/m. This finding should be very helpful for structural engineers in regards to their consideration of durability design of RC structures. Nevertheless, more simulations will be ideal in the future for some extra clarification; for example, more values of spacing between reinforcements.

6.4 Crack path

To investigate the change of normal stress (crack driving force) of the cohesive elements along the cracks over time, Figures 21 and 22 are plotted for the side crack and the top crack respectively. The spacing between reinforcements is taken 30 mm and the fracture energy is 120 N/m. The normal stress distributions of cohesive elements along the side crack are shown for 0.12 year, 1.13 years and 10 years in Figure 21. There are 19 elements in the path of side crack and the elements are ordered from the surface of concrete to the inner boundary. At 0.12 year, the first element (no. 19) from the inner boundary approaches the tensile strength. As the load increases, the side crack is initiated and the peak stress moves along the crack path towards the surface. At 1.13 year, the peak stress moves to the location of element no. 4 while the normal stresses for all previously cracked cohesive elements soften/degrade to certain values, according to its constitutive stress-displacement ration defined in Figure 3. For this example, because of the existence of top crack, the surface region of the side crack is always in compression as shown in Figure 12. Even at 10 years, the side crack tip can only reach the cohesive element no. 2 whilst the first cohesive element from the surface is in significant compression, more than 10 MPa. This reflects complex nature of the problem for non-uniform corrosion of multiple reinforcing bars.

Figure 22 shows the normal stress distributions of cohesive elements along the top crack under the case of reinforcement spacing 30 mm and fracture energy 120 N/m. It can be seen that the peak tensile stress moves from the cohesive element no. 21 (at the top surface) to the cohesive element no. 2 (close to the inner boundary), as time increases. At 0.12 year, the concrete near reinforcing bar is in compression while the concrete near the surface of concrete is in tension. As explained earlier, this is why the top crack is initiated at the top, rather than at the inner boundary. From 0.12 to 1.43 years, the top crack propagates fast, i.e., the peak tensile stress moves from cohesive element no. 21 to no. 6; the location of peak tensile stress is usually referred to as the start of fracture process zone or the fictitious crack front, according to definition of cohesive crack model [40].

7 CONCLUSIONS

A combined analytical and numerical method has been presented to predict the time to cover cracking and the crack width under non-uniform corrosion of multiple reinforcing bars of RC structures. The non-uniform corrosion model was derived based on experimental results and formulated as a function of time. Under the non-uniform corrosion-induced expansion, a fracture model was established to simulate arbitrary cracking of the cover of RC structures with multiple reinforcing bars. The times to cracking and failure modes of concrete cover affected by fracture energy of concrete and spacing between reinforcing bars were obtained and discussed. To validate the developed model, comparisons with experimental results from literature were carried out. It has been found that the time to surface cracking is significantly affected by ambient temperature, chloride content and corrosion rate. It has also been found that two cover failure modes exist, depending on the spacing of reinforcing bars and fracture energy of concrete. It can be concluded that the developed combined analytical and numerical model can be used to accurately simulate the time to cover cracking and the crack width evolution of RC structures caused by non-uniform corrosion of multiple reinforcing bars.

ACKNOWLEDGEMENT

Financial support from National Key R&D Plan of China (Grant No: 2016YFC0600801) is gratefully acknowledged. The first author is also funded by China Scholarship Council for his PhD research at University of Strathclyde, UK.

REFERENCES

[1] C. Q. Li, and S. T. Yang, "Prediction of concrete crack width under combined reinforcement corrosion and applied load," *Journal of Engineering Mechanics-ASCE,* vol. 137, no. 11, pp. 722-731, 2011.

[2] Y. Liu, and R. E. Weyers, "Modelling the time-to-corrosion cracking in chloride contaminated reinforced concrete structures," *ACI Materials Journal,* vol. 95, no. 6, pp. 675-681, 1998.

[3] K. Bhargava, A. K. Ghosh, Y. Mori *et al.*, "Model for cover cracking due to rebar corrosion in RC structures," *Engineering Structures,* vol. 28, no. 8, pp. 1093-1109, 2006.

[4] S. J. Pantazopoulou, and K. D. Papoulia, "Modeling cover cracking due to reinforcement corrosion in RC structures," *Journal of Engineering Mechanics-ASCE,* vol. 127, no. 4, pp. 342-351, 2001.

[5] M. Elices, C. Rocco, and C. Roselló, "Cohesive crack modelling of a simple concrete: Experimental and numerical results," *Engineering Fracture Mechanics,* vol. 76, no. 10, pp. 1398-1410, 2009.

[6] C. Andrade, C. Alonso, and F. J. Molina, "Cover cracking as a function of bar corrosion: Part I-Experimental test," *Materials and Structures,* vol. 26, no. 8, pp. 453-464, 1993.

[7] C. Q. Li, "Time Dependent Reliability Analysis of the Serviceability of Corrosion Affected Concrete Structures," *International Journal of Materials and Structural Reliability,* vol. 3, no. 2, pp. 105-116, 2005.

[8] L. Chernin, and D. V. Val, "Prediction of corrosion-induced cover cracking in reinforced concrete structures," *Construction and Building Materials,* vol. 25, no. 4, pp. 1854-1869, 2011.

[9] C. Q. Li, R. E. Melchers, and J. J. Zheng, "Analytical model for corrosion-induced crack width in reinforced concrete structures," *ACI Structural Journal,* vol. 103, no. 4, pp. 479-487, 2006.

[10] L. Jin, R. Zhang, X. Du *et al.*, "Investigation on the cracking behavior of concrete cover induced by corner located rebar corrosion," *Engineering Failure Analysis,* vol. 52, pp. 129-143, 2015.

[11] E. Chen, and C. K. Y. Leung, "Finite element modeling of concrete cover cracking due to non-uniform steel corrosion," *Engineering Fracture Mechanics,* vol. 134, pp. 61-78, 2015.

[12] C. Cao, and M. M. S. Cheung, "Non-uniform rust expansion for chloride-induced pitting corrosion in RC structures," *Construction and Building Materials,* vol. 51, pp. 75-81, 2014.

[13] K. A. T. Vu, and M. G. Stewart, "Structural reliability of concrete bridges including improved chloride-induced corrosion models," *Structural Safety,* vol. 22, no. 4, pp. 313-333, 2000.

[14] M. G. Stewart, "Spatial variability of pitting corrosion and its influence on structural fragility and reliability of RC beams in flexure," *Structural Safety,* vol. 26, no. 4, pp. 453-470, 2004.

[15] J. A. González, C. Andrade, C. Alonso *et al.*, "Comparison of rates of general corrosion and maximum pitting penetration on concrete embedded steel reinforcement," *Cement and Concrete Research,* vol. 25, no. 2, pp. 257-264, 1995.

[16] Y. Yuan, and Y. Ji, "Modeling corroded section configuration of steel bar in concrete structure," *Construction and Building Materials,* vol. 23, no. 6, pp. 2461-2466, 2009.

[17] B. S. Jang, and B. H. Oh, "Effects of non-uniform corrosion on the cracking and service life of reinforced concrete structures," *Cement and Concrete Research,* vol. 40, no. 9, pp. 1441-1450, 2010.

[18] B. Šavija, M. Luković, J. Pacheco *et al.*, "Cracking of the concrete cover due to reinforcement corrosion: A two-dimensional lattice model study," *Construction and Building Materials,* vol. 44, pp. 626-638, 2013.

[19] A. Chen, Z. Pan, and R. Ma, "Mesoscopic simulation of steel rebar corrosion process in concrete and its damage to concrete cover," *Structure and Infrastructure Engineering,* vol. 13, no. 4, pp. 478-493, 2016.

[20] Y. Zhao, A. R. Karimi, H. S. Wong *et al.*, "Comparison of uniform and non-uniform corrosion induced damage in reinforced concrete based on a Gaussian description of the corrosion layer," *Corrosion Science,* vol. 53, no. 9, pp. 2803-2814, 2011.

[21] Z. P. Bazant, "Physical model for steel corrosion in concrete sea structures - theory," *Journal of the Structural Division-ASCE,* vol. 105, no. 6, pp. 1137-1153, 1979.

[22] C. Andrade, F. J. Molina, and C. Alonso, "Cover cracking as a function of rebar corrosion: Part 1-experiment test," *Materials and Structures,* vol. 26, pp. 453-454, 1993.

[23] C. Lu, W. Jin, and R. Liu, "Reinforcement corrosion-induced cover cracking and its time prediction for reinforced concrete structures," *Corrosion Science,* vol. 53, no. 4, pp. 1337-1347, 2011.

[24] C. Cao, M. M. S. Cheung, and B. Y. B. Chan, "Modelling of interaction between corrosion-induced concrete cover crack and steel corrosion rate," *Corrosion Science,* vol. 69, pp. 97-109, 2013.

[25] Y. Yuan, Y. Ji, and J. Jiang, "Effect of corrosion layer of steel bar in concrete on time-variant corrosion rate," *Materials and Structures,* vol. 42, no. 10, pp. 1443-1450, 2009.

[26] Y. Yuan, J. Jiang, and T. Peng, "Corrosion process of steel bar in concrete in full lifetime," *ACI Materials Journal,* vol. 107, no. 6, pp. 562-568, 2010.

[27] J. Jiang, and Y. Yuan, "Prediction model for the time-varying corrosion rate of rebar based on micro-environment in concrete," *Construction and Building Materials,* vol. 35, pp. 625-632, 2012.

[28] J. Jiang, and Y. Yuan, “Development and prediction strategy of steel corrosion rate in concrete under natural climate,” *Construction and Building Materials,* vol. 44, pp. 287-292, 2013.

[29] X. Du, L. Jin, and R. Zhang, “Modeling the cracking of cover concrete due to non-uniform corrosion of reinforcement,” *Corrosion Science,* vol. 89, pp. 189-202, 2014.

[30] A. Jamali, U. Angst, B. Adey *et al.*, “Modeling of corrosion-induced concrete cover cracking: A critical analysis,” *Construction and Building Materials,* vol. 42, pp. 225-237, 2013.

[31] J. Zhang, X. Ling, and Z. Guan, “Finite element modeling of concrete cover crack propagation due to non-uniform corrosion of reinforcement,” *Construction and Building Materials,* vol. 132, pp. 487-499, 2017.

[32] K. Vu, M. G. Stewart, and J. Mullard, “Corrosion-induced cracking: Experimental data and predictive models,” *ACI Structural Journal,* vol. 102, no. 5, pp. 719-726, 2005.

[33] W. Jung, “Predicting the remaining service life of land concrete by steel corrosion,” *Cement and Concrete Research,* vol. 33, no. 5, pp. 663-677, 2003.

[34] R. Zhang, A. Castel, and R. François, “The corrosion pattern of reinforcement and its influence on serviceability of reinforced concrete members in chloride environment,” *Cement and Concrete Research,* vol. 39, no. 11, pp. 1077-1086, 2009.

[35] D. Chen, and S. Mahadevan, “Chloride-induced reinforcement corrosion and concrete cracking simulation,” *Cement and Concrete Composites,* vol. 30, no. 3, pp. 227-238, 2008.

[36] Metoffice.uk, "UK temperature, rainfall and sunshine anomaly graphs," http://www.metoffice.gov.uk/climate/uk/summaries/datasets, 2017.

[37] A. S. Al-Harthy, M. G. Stewart, and J. Mullard, “Concrete cover cracking caused by steel reinforcement corrosion,” *Magazine of Concrete Research,* vol. 63, no. 9, pp. 655-667, 2011.

[38] J. A. Mullard, and M. G. Stewart, “Corrosion-induced cover cracking: new test data and predictive models,” *ACI Structural Journal,* vol. 108, no. 1, pp. 71-79, 2011.

[39] S. Caré, Q. T. Nguyen, K. Beddiar *et al.*, “Times to cracking in reinforced mortar beams subjected to accelerated corrosion tests,” *Materials and Structures,* vol. 43, no. 1-2, pp. 107-124, 2009.

[40] A. Hillerborg, M. Modeer, and P. E. Petersson, “Analysis of crack formation and crack growth in concrete by means of fracture mechanics and finite elements,” *Cement and Concrete Research,* vol. 6, no. 6, pp. 773-781, 1976.

[41] C. Q. Li, “Life-cycle modelling of corrosion-affected concrete structures: Propagation,” *Journal of Structural Engineering-ASCE* vol. 129, no. 6, pp. 753-761, 2003.

[42] S. P. Timoshenko, and J. N. Goodier, *Theory of Elasticity*, 3rd ed., Singapore, 1970.

[43] X. Shilang, *Determination of parameters in the bilinear,Reinhardt’s nonlinear and exponentially non-linear softening curves and their physical meanings*, University of Stuttgart, Stuttgart, 1999.

[44] S. Xu, and X. Zhang, “Determination of fracture parameters for crack propagation in concrete using an energy approach,” *Engineering Fracture Mechanics,* vol. 75, no. 15, pp. 4292-4308, 2008.

LIST OF TABLES

Table 1 The average monthly temperature in England from 1996-2016 (°C) [36]

Jan.	Feb.	Mar.	Apr.	May.	Jun.	Jul.	Aug.	Sept.	Oct.	Nov.	Dec.
4.41	4.70	6.32	8.66	11.57	14.38	16.37	16.34	14.21	10.90	7.18	4.75

Table 2 Values of basic variables used in the time-dependent non-uniform corrosion model

Symbol	Values	Sources
D	12 mm	Li [41]
d_0	0.0125 mm	Liu and Weyers [2]
α_{rust}	0.57	Liu and Weyers [2]
ρ_{rust}	3.60 mg/mm^3	Liu and Weyers [2]
ρ_{st}	7.85 mg/mm^3	Liu and Weyers [2]
W_{rust}	mg	Liu and Weyers [2]
w/c	0.54	Jiang [27]
Cl^-	3.034%	Jiang [27]
P	0.68	Jiang [27]
T_{t_1}	289.36 K	Metoffice.uk[36]

Table 3 Values for geometric and mechanical parameters in cracking simulation

Description	Symbol	Values
Cover thickness	C	20 mm
Clear space of steel bars	S	30 mm 45 mm 60 mm
Diameter of steel bars	D	12 mm
Length of RC	L	178 mm
Height of RC	H	400 mm
Effective modulus of elasticity	E_{ef}	18.82 GPa [41]
Poisson's ratio	ν_c	0.18 [41]
Shear modulus	G	$E/[2(1+\nu)]$ [42]
Tensile strength	$f_t^{'}$	5.725 MPa [41]
Fracture energy	G_f	60 N/m [43, 44] 90 N/m [43, 44] 120 N/m [43, 44]

Table 4 Crack patterns and time to cracking for different values of fracture energy and reinforcement clear spacing

	G_{f1}							G_{f2}							G_{f3}						
	P	t_{th1}	t_{th2}	t_{to1}	t_{to2}	t_{si1}	t_{si2}	P	t_{th1}	t_{th2}	t_{to1}	t_{to2}	t_{si1}	t_{si2}	P	t_{th1}	t_{th2}	t_{to1}	t_{to2}	t_{si1}	t_{si2}
S_1	*De*	0.41	0.44	N/A	N/A	0.60	0.85	*De*	0.62	0.70	N/A	N/A	0.91	1.05	*Sp*	0.86	0.92	1.43	N/A	1.13	N/A
S_2	*Sp*	0.62	0.79	0.70	N/A	0.62	N/A	*Sp*	0.89	0.93	0.89	N/A	1.01	N/A	*Sp*	1.04	1.11	1.64	N/A	1.33	N/A
S_3	*Sp*	0.67	1.3	0.70	N/A	0.67	N/A	*Sp*	0.88	1.59	0.84	N/A	1.00	N/A	*Sp*	1.13	1.88	1.04	N/A	1.46	N/A

Parameter	Description or value
G_{f1}	Fracture energy 60 N/m
G_{f2}	Fracture energy 90 N/m
G_{f3}	Fracture energy 120 N/m
S_1	Spacing between rebars 30 mm
S_2	Spacing between rebars 45 mm
S_3	Spacing between rebars 60 mm
P	Crack pattern
De	Delamination
Sp	Combined delamination and corner spalling
t_{th1}	Time to initiation of through crack
t_{th2}	Time to complete formation of through crack
t_{to1}	Time to initiation of top crack
t_{to2}	Time to complete formation of top crack
t_{si1}	Time to initiation of side crack
t_{si2}	Time to complete formation of side crack
Time unit	year

Table 5 Values for basic variables used for validation

Description	**Symbol**	**Values**
Top cover thickness	C_T	20 mm
Edge cover thickness	C_E	75 mm
Space of steel bars	S	150 mm
Diameter of steel bars	D	12 mm
Length of RC	L	648 mm
Height of RC	H	400 mm
Effective modulus of elasticity	E_{ef}	18.82 GPa
Poisson's ratio	ν_c	0.18
Tension strength	$f_t^{'}$	2.4 MPa
Fracture energy	G_f	65 N/m
Corrosion rate	i_{corr}	100 μA/cm^2

LIST OF FIGURES

21. Normal stress distributions along the side crack

22. Normal stress distributions along the top crack

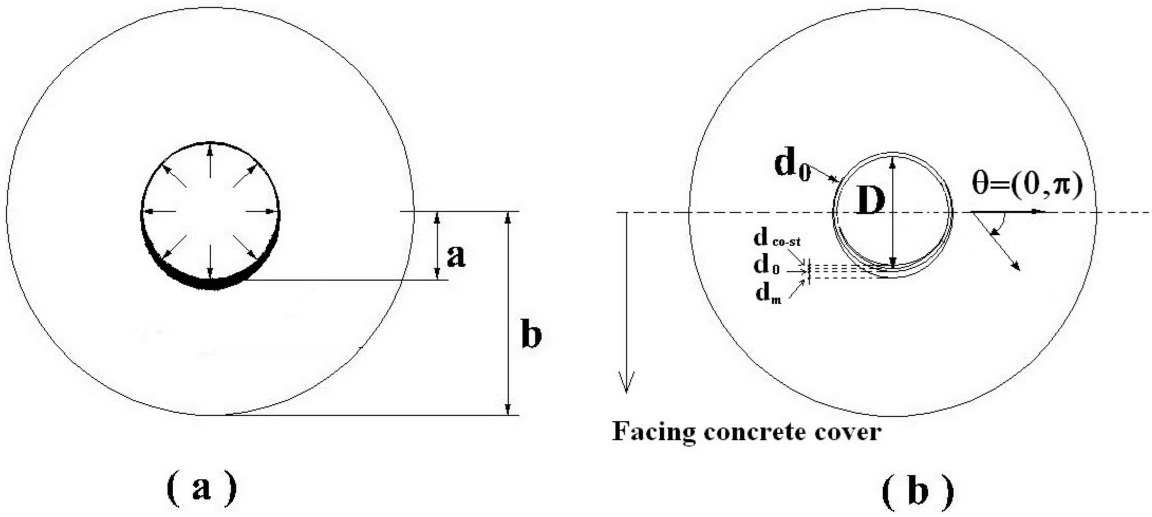

Figure 1 Non-uniform corrosion model

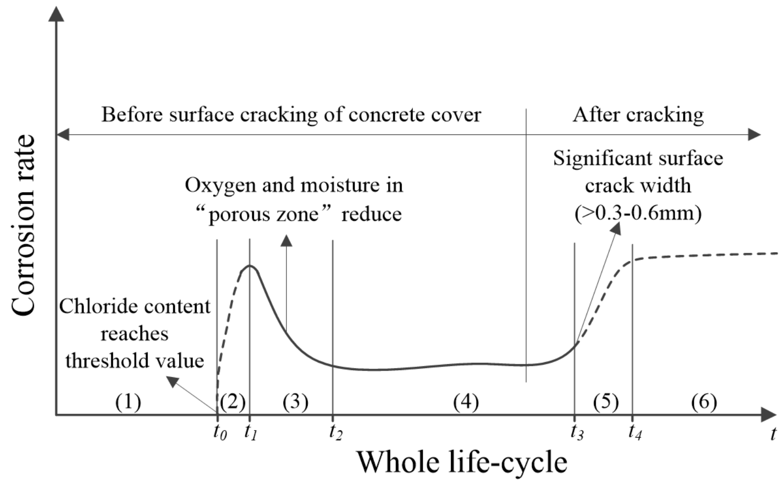

Figure 2 Time-dependent corrosion rate in the whole life-cycle of RC structures

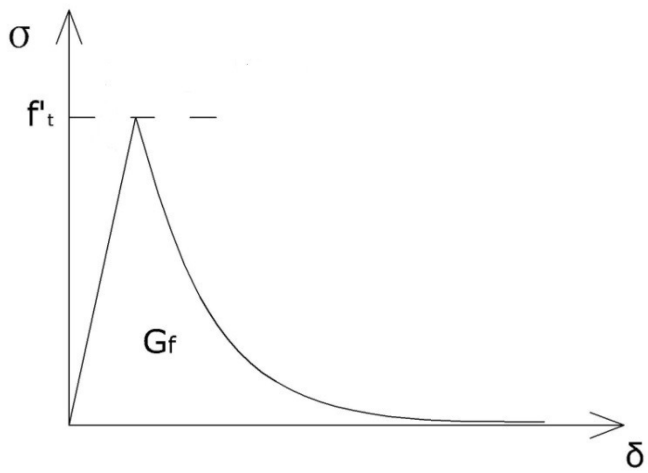

Figure 3 Constitutive relationship of concrete in tension for Mode-I fracture

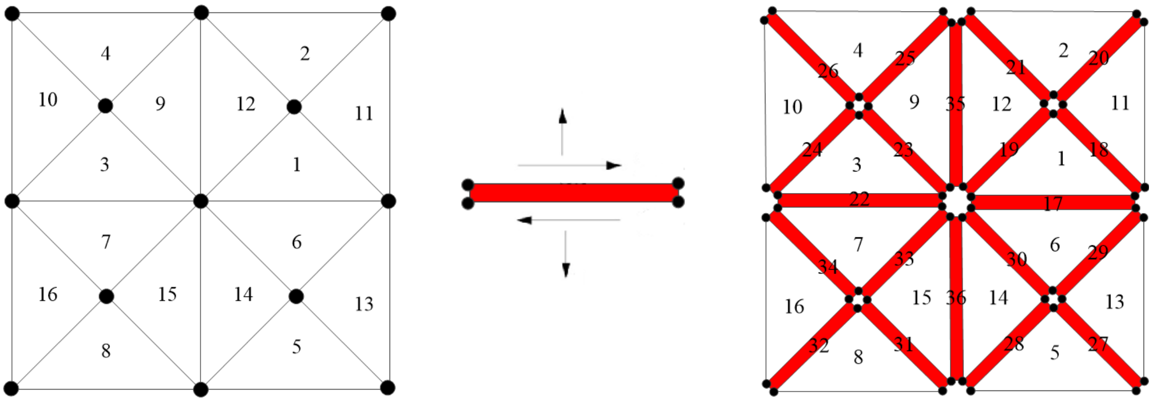

(a) (b) (c)

Figure 4 Insertion process of cohesive elements: (a) initial mesh; (b) inserted cohesive element based on newly created nodes; and (c) mesh after insertion of cohesive elements

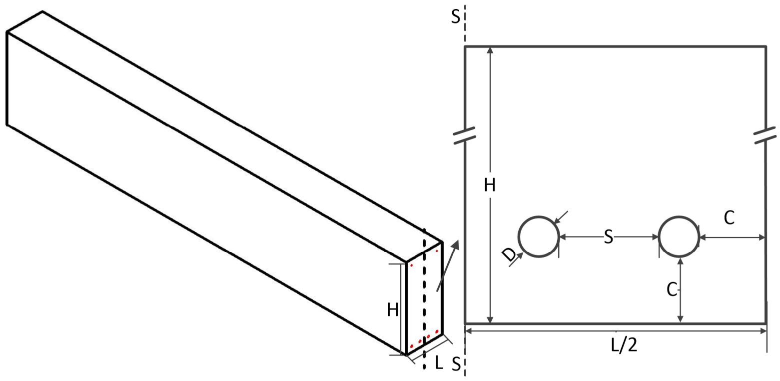

Figure 5 Configuration of the RC beam with multiple tension bars

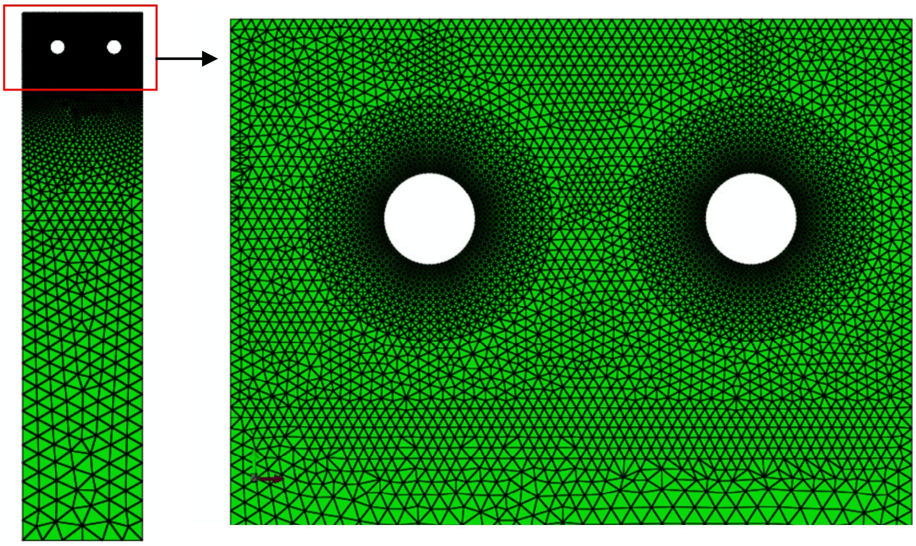

Figure 6 Typical meshing for half of the cover structure modelled

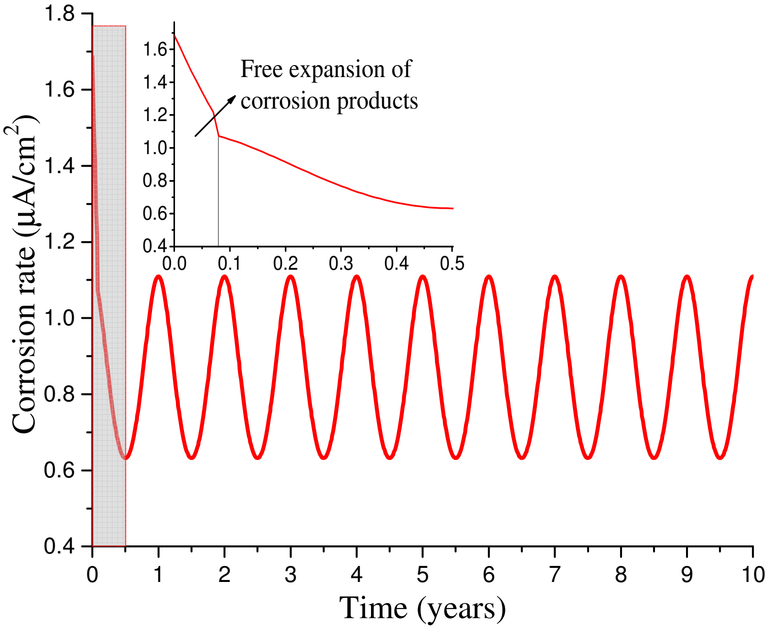

Figure 7 Time-dependent corrosion rate from corrosion initiation by considering seasoned effect

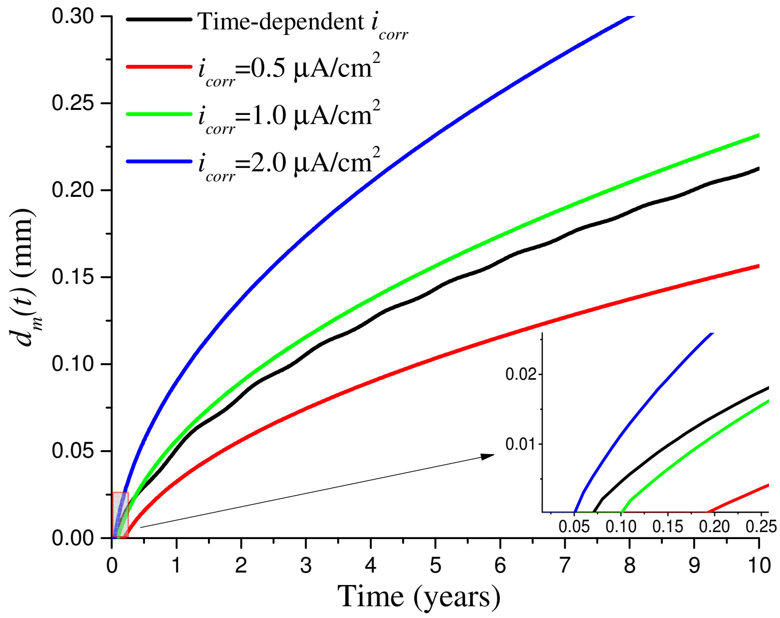

Figure 8 Development of $d_m(t)$ as a function of time under various corrosion rates

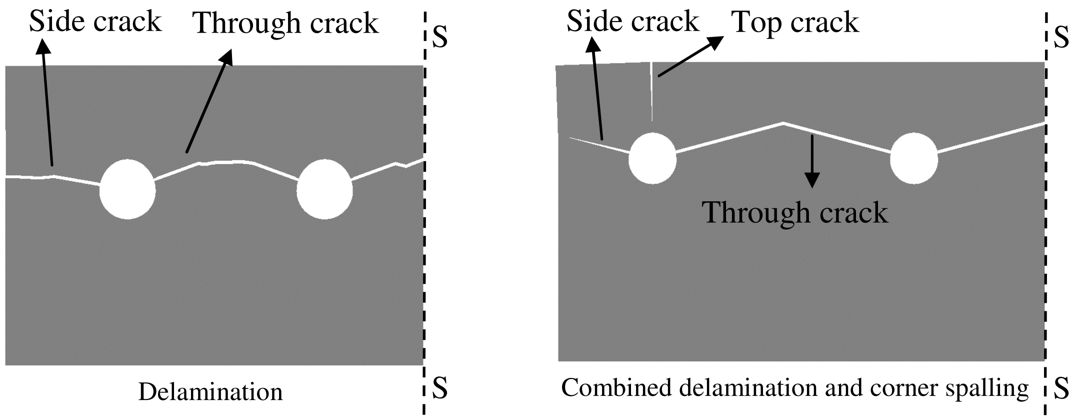

Figure 9 Two typical cracking patterns for half of RC structures

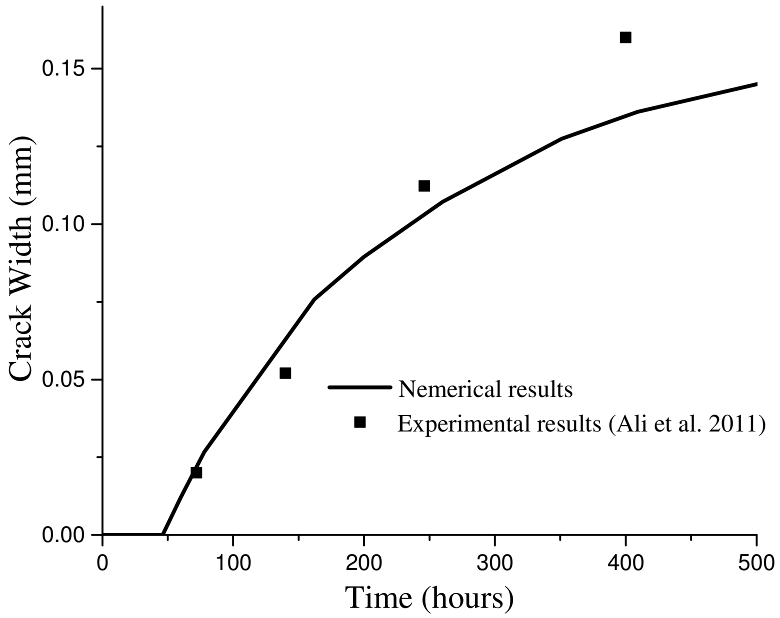

Figure 10 Experimental verification of the crack width

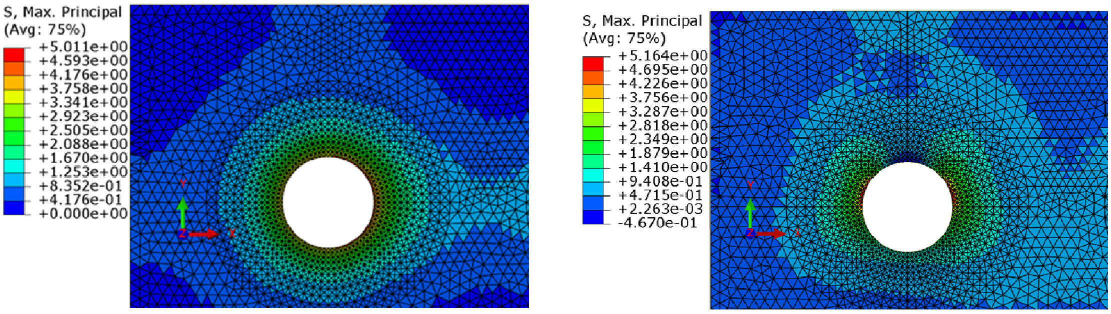

(a) (b)

Figure 11 The maximum principal stress distributions around the corner rebar under (a) uniform corrosion and (b) non-uniform corrosion

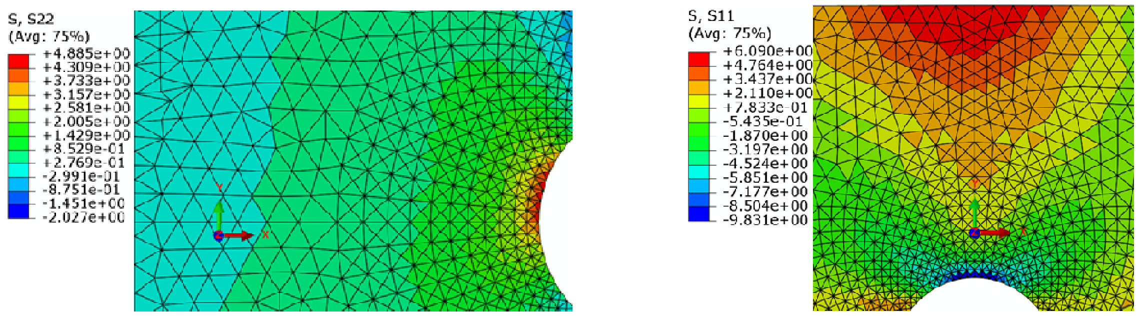

(a) (b)

Figure 12 Normal (driving) stress distributions of (a) side crack and (b) top crack prior to cracking initiation

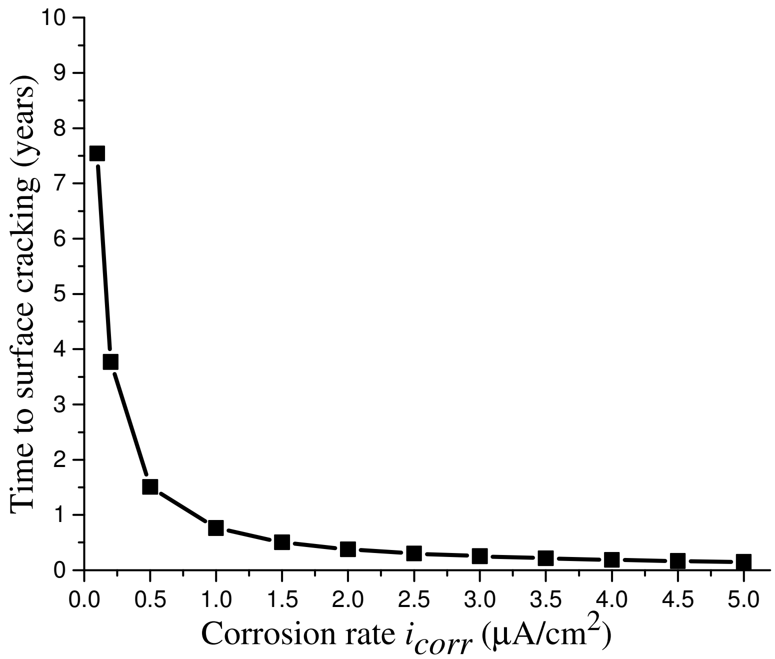

Figure 13 Time to surface cracking (top crack) as a function of corrosion rate

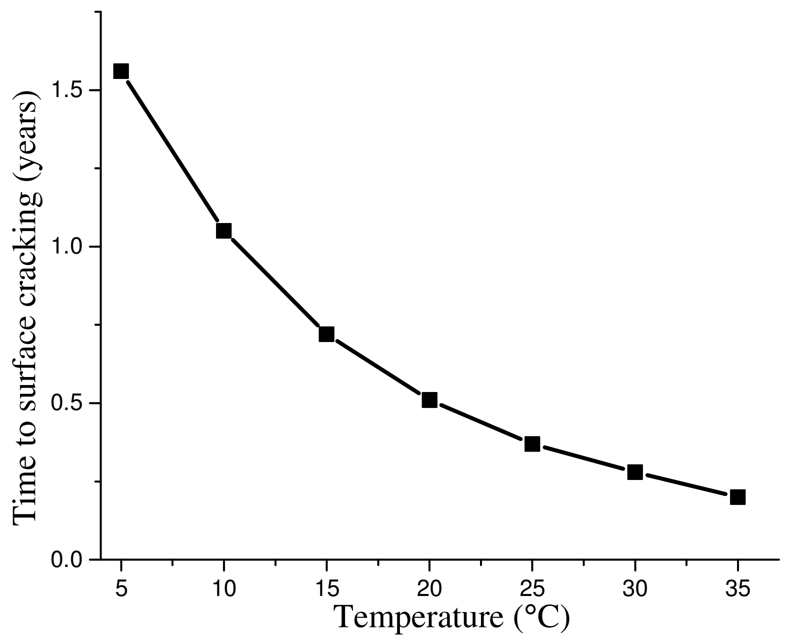

Figure 14 Time to surface cracking (top crack) as a function of ambient temperature

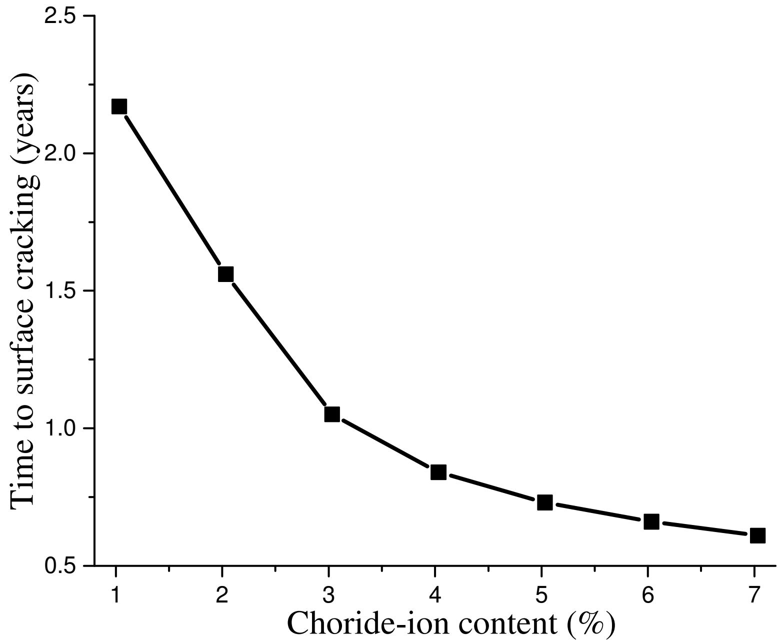

Figure 15 Time to surface cracking (top crack) as a function of chloride-ion content

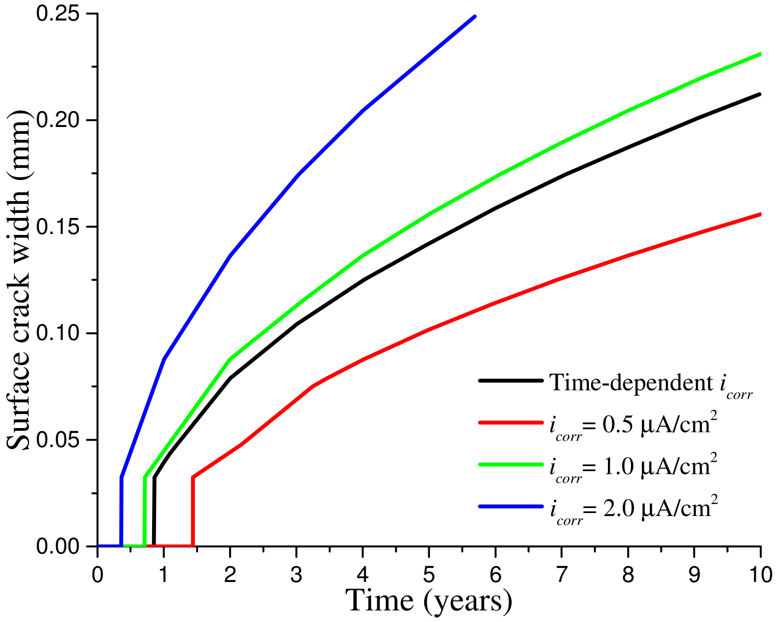

Figure 16 Surface crack width (top crack) as a function of time under various corrosion rates

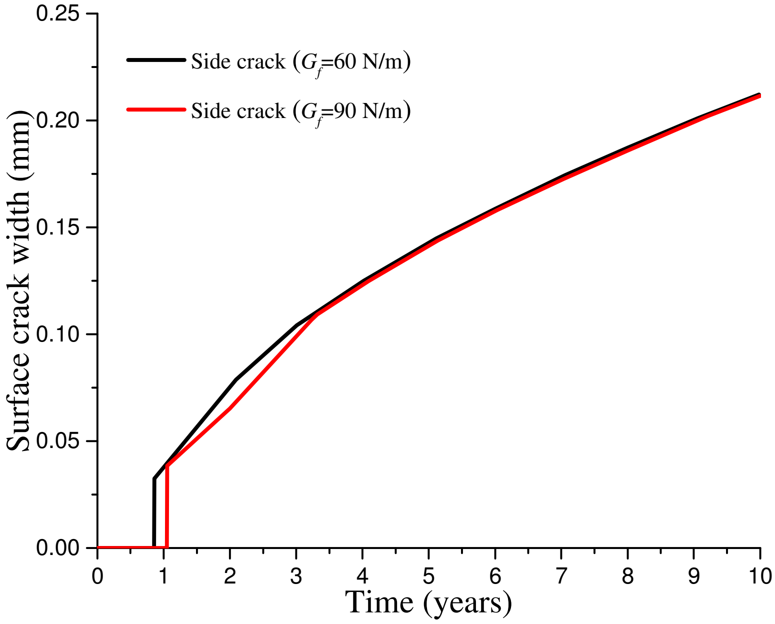

Figure 17 Surface crack width (side crack) as a function of time for different fracture energies of concrete

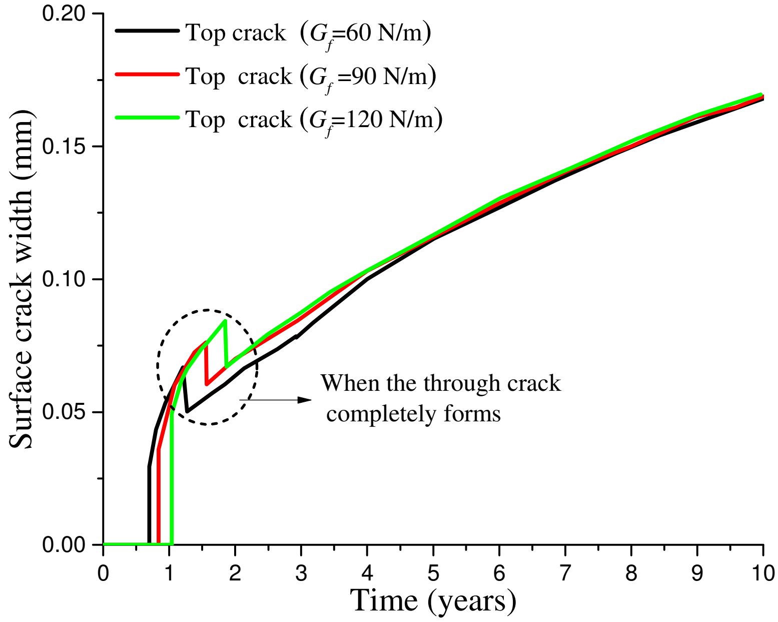

Figure 18 Surface crack width (top crack) as a function of time for different fracture energies of concrete

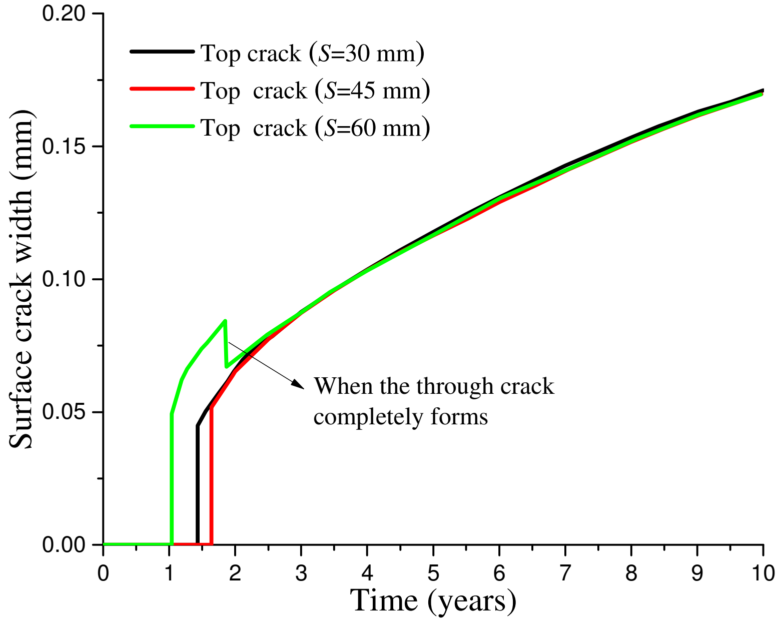

Figure 19 Surface crack width (top crack) as a function of time for different reinforcement spacing

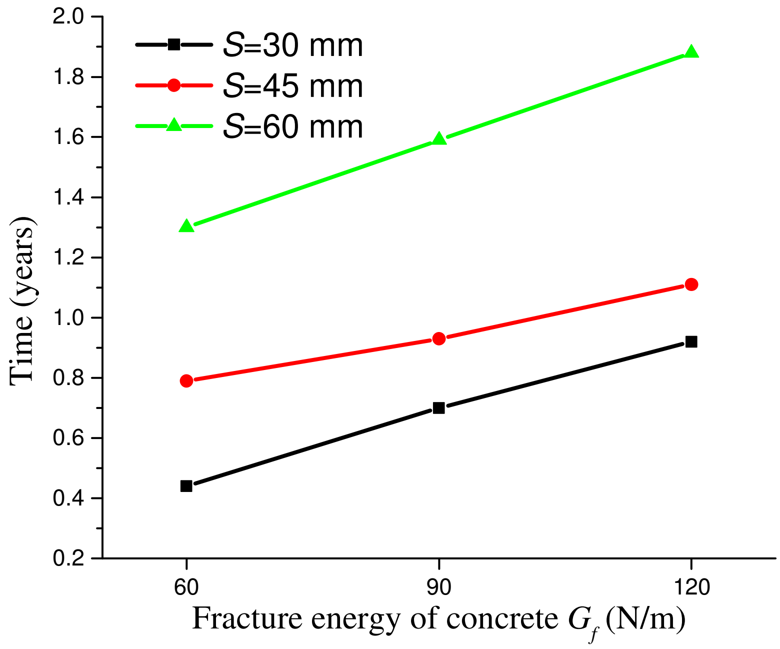

(a) Time to complete formation of through crack

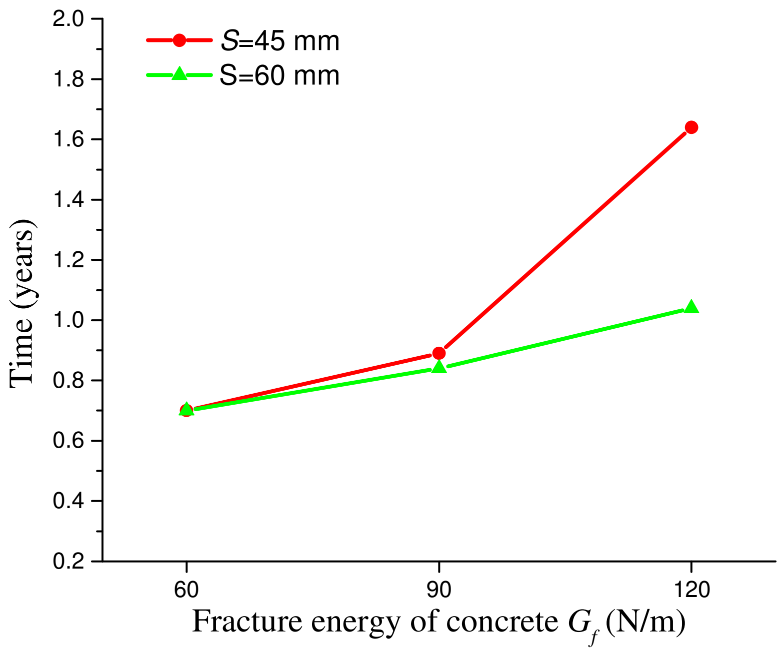

(b) Time to initiation of top surface crack

Figure 20 Effect of fracture energy and spacing on time to cracking

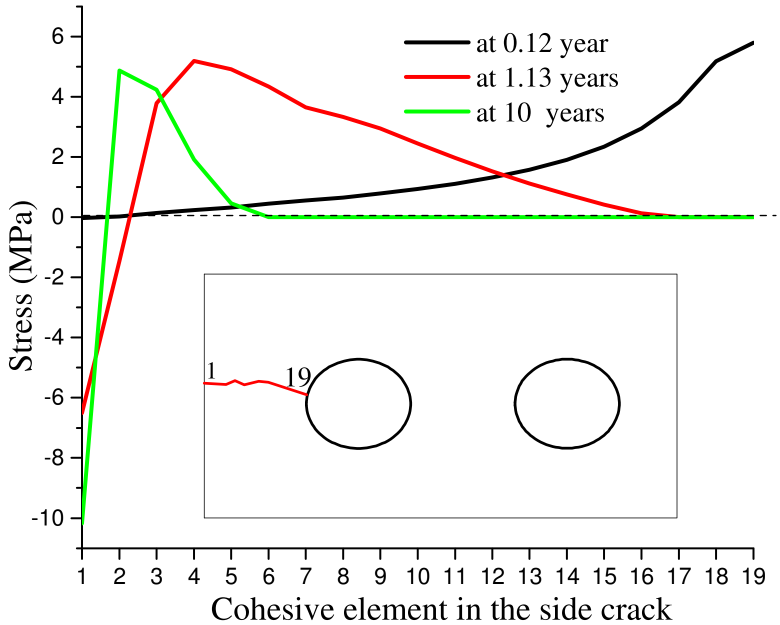

757

758 Figure 21 Normal stress distributions along the side crack

759

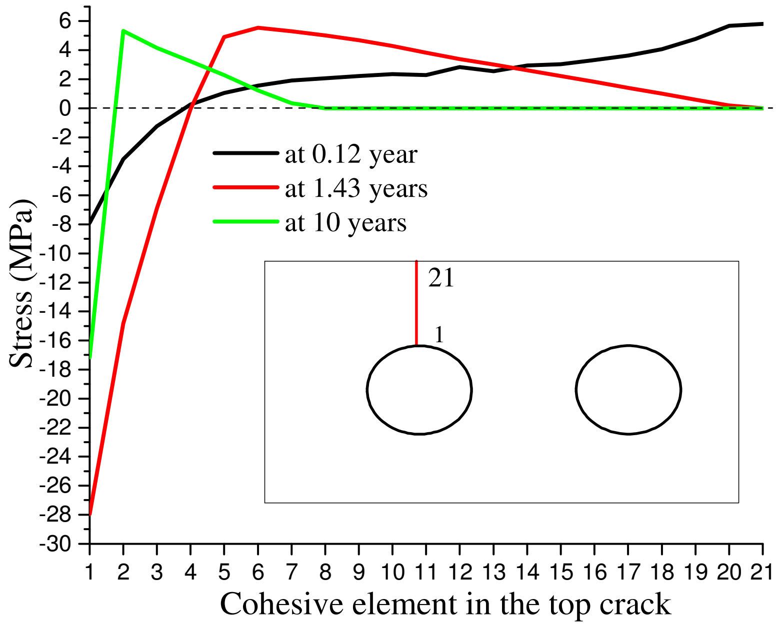

Figure 22 Normal stress distributions along the top crack